ACS Sustainable Chemistry & Engineering

pubs.acs.org/journal/ascecg

Research Article

Valorization of Refined Lignin Fractions as Green Promoters in Photochemical Atom Transfer Radical Addition Reactions

Claudio Gioia,* Vasco Corti, Alessandro Filippini, Dario Zanichelli, Francesco Palazzi, Pavel Solovyev, Maurizio Prato, and Giacomo Filippini*

Cite This: *ACS Sustainable Chem. Eng.* 2025, 13, 12300−12310

Read Online

ACCESS | Metrics & More | Article Recommendations | Supporting Information

ABSTRACT: Herein, we report a novel green photochemical procedure for the direct functionalization of terminal olefins with radical precursors promoted by technical lignin architectures. Spruce Kraft lignin was initially subjected to solvent refining to achieve fractions presenting a controlled molecular weight and fully characterized structural features. The obtained fractions were then tested as photoinitiators for organic transformations under visible light irradiation. The results demonstrated that a low molecular weight refined lignin, namely, **L**-EtOAc, was able to successfully promote relevant photoinduced radical reactions, providing several densely functionalized alkyl halides (14 examples, up to 98% yield). Mechanistic investigations were also performed to understand the role of lignin architecture in the reaction pathway. This work proposes an innovative role for lignin in organic chemistry, laying the basis for a brand-new field for the valorization of cheap technical lignocellulosic byproducts, while opening new exciting scenarios concerning green photochemical processes.

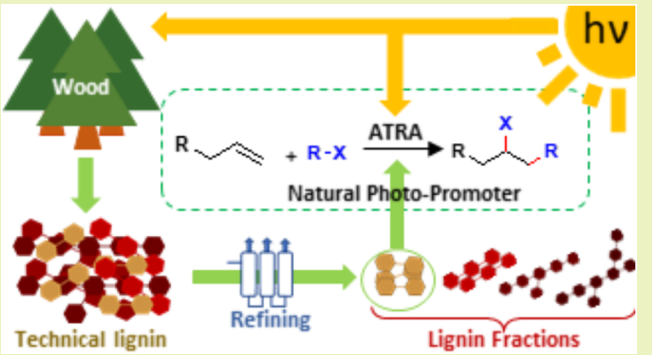

KEYWORDS: *lignin, synthetic methods, photochemistry, radical reactions, C−C coupling*

1. INTRODUCTION

Atom transfer radical addition (ATRA) reactions are simple, robust, and atom-economical strategies to prepare valuable alkyl halides.[1,2] The overall process involves the addition of a suitable radical precursor (R−X) to an unsaturated hydrocarbon, thus creating both a new C−C and C−X bond (where X is a halogen atom) in one synthetic step.[2] From a mechanistic point of view, the ATRA reaction generally proceeds through a radical chain propagation manifold. Since the groundbreaking work of Kharasch, organic chemists have developed a large number of approaches to initiate the ATRA mechanism.[3−13] More specifically, the radical initiation step may be achieved through two general activation modes: (i) thermal activation or (ii) photochemical activation. Originally, the homolytic cleavage of the C−X bond, within the radical precursor, was achieved by exploiting harsh reaction conditions, such as high temperatures or high-energy ultraviolet-light (UV-light) irradiation.[13,14] Subsequently, potential explosive radical initiators (*e.g.*, organic peroxides and azonitriles) or harmful metal-based promoters have been employed for this purpose.[15,16] In recent years, novel photochemical and photocatalytic methods have been designed to initiate ATRA reactions under ultraviolet-visible (UV−vis) light irradiation.[17,18] In this context, precious and potentially toxic metal complexes, substoichiometric amounts of organic chromophores, and photoactive (nano)materials have been effectively exploited.[19−32] Because of this, the general feeling is that the advance within this research field would require the development of novel, efficient, inexpensive, and safe photoinitiators capable of working under visible light irradiation.[33−39] Moreover, it is worth mentioning that these metal-free photoactive promoters must be readily available on a large scale to allow their industrial application. Fully feeding into the current green transition principles, a further improvement for photochemical ATRA reactions would be centered on the exploitation and valorization of natural architectures deriving from agro-forestry byproducts. Among all-natural architectures, lignin represents an excellent choice for designing novel green photochemical transformations. Indeed, lignin constitutes a ubiquitous byproduct of the paper and ethanol industry with an overall world production of about 100 million tonnes/per year.[40−42] Lignin structure mainly derives from the biologically driven radical reactions of unsaturated phenols, among which *p*-coumaryl alcohol, coniferyl alcohol, and synapyl alcohol constitute the majority.

Received: May 31, 2025
Revised: July 11, 2025
Accepted: July 14, 2025
Published: July 23, 2025

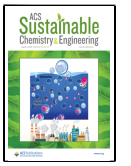

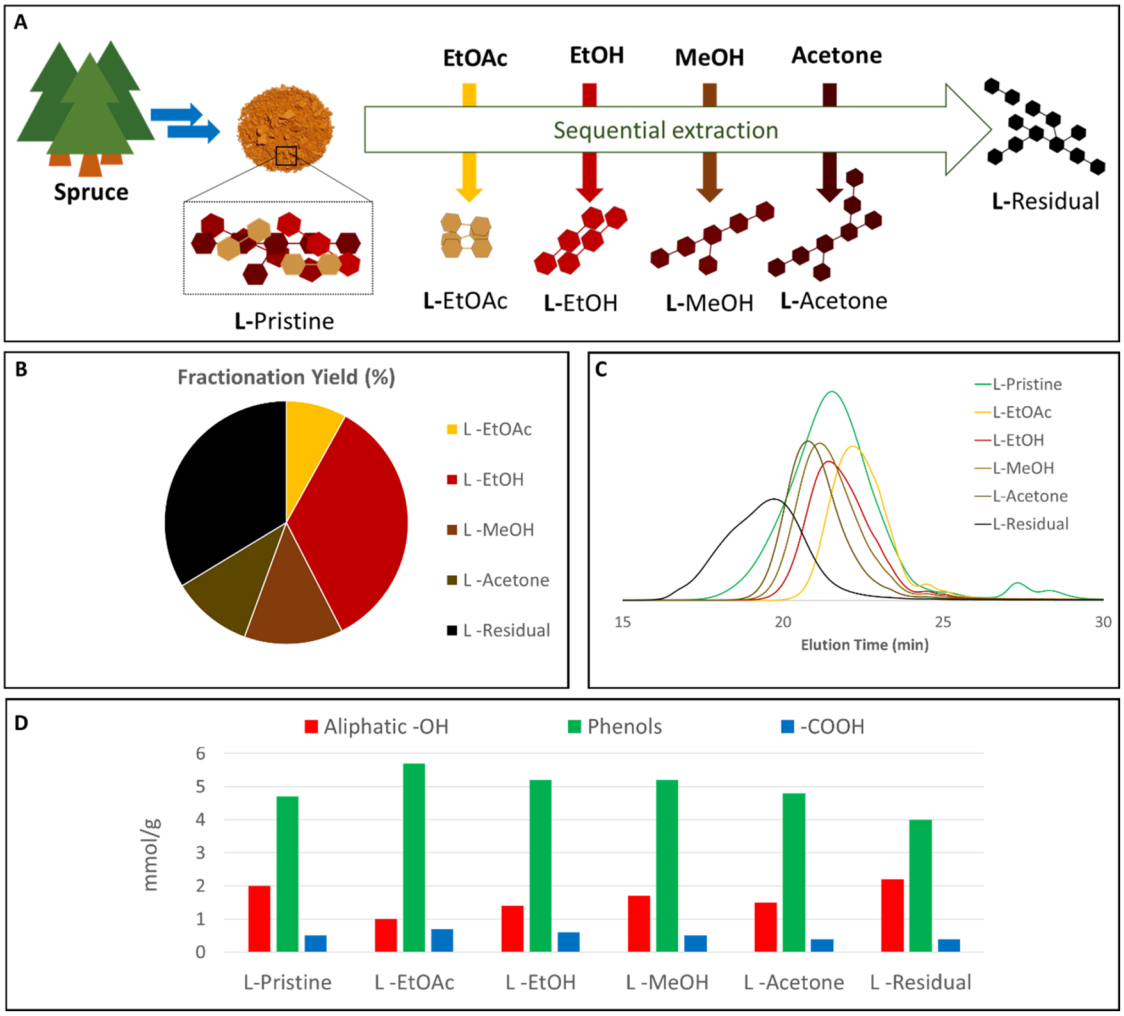

Figure 1. (A) Lignin refining approach by sequential solvent extraction. (B) Fractionation yields. (C) Molecular weight distribution of the obtained fractions determined by size exclusion chromatography (SEC) using a SEC 1260 infinity (Polymer standard service, Germany) equipped with a PSS precolumn, PSS column 100 Å, and PSS GRAM 10,000 Å analytical columns thermostated at 60 °C; the calibration plot was constructed with pullulan standards. (D) Main reactive functional groups were determined by ^{31}P NMR.

In particular, the radical polymerization, controlled by the vegetal cells, produces a complex tridimensional structure able to embed cellulose and confer stability and protection to the entire plant.[43,44] Lignin, usually isolated from the black liquor resulting from the cellulose extraction process, appears as a mixture of aromatic architectures, presenting a huge variety in terms of composition, chemical connectivity, molecular weight, and functionalities. In particular, the presence of phenylpropane units, conjugated double bonds, quinone, and chalcone structures is mainly responsible for the lignin substantial UV absorption within the wavelength range of 250−400 nm, while aggregated-induced emissions affect mainly its fluorescent character.[45−50] In particular, lignin exhibits a primary absorbance which is mainly attributed to the $\pi-\pi^*$ transitions of the aromatic structural units and the $n-\pi^*$ transitions of the carbonyl groups directly bounded to aromatics.[51−53] While on one hand, such a plethora of structural features is allowing lignin to emerge as a promising UV blocker in materials science,[54−57] on the other, its diversity in functionality and molecular weight are detrimental to its involvement in valuable fields such as photoreaction promotion. In recent years, lignin and its derivatives have been effectively employed as components for the production of novel photoactive materials (*e.g.*, composites, nanostructures and supramolecular hydrogels) that showed to be capable to drive the synthesis of valuable chemicals, including polyolefins and H_2O_2.[58−60] In this context, the implementation of refining processes would be beneficial in overcoming technical lignin variability, producing more homogeneous fractions in terms of molecular weight and functionality. This approach was successfully exploited for the application of lignin as an antioxidant,[61−64] pollutant absorber,[65,66] and constituent of thermosetting materials, improving reproducibility and the understanding of the lignin structure on performance.[67−71] Here is proposed a new method to valorize lignin as a novel photochemical promoter in ATRA reactions between terminal olefins and suitable radical precursors. Initially, technical lignin has been refined to achieve fully characterized, reproducible fractions presenting a controlled molecular weight. The resulting fractions were then tested as photoinitiators in a model ATRA transformation. While optimizing the methodology, the role of lignin architecture and the impact of its chemical structure have been assessed to better understand the main aspects regulating the reaction and its application on a wide range of substrates. Lastly, a mechanism for the lignin-promoted photochemical reaction has been proposed. We

https://doi.org/10.1021/acssuschemeng.5c05307
ACS Sustainable Chem. Eng. 2025, 13, 12300−12310

Table 1. Overview of the Fractionation: Main Functional Groups, Molecular Weight, and Yield

lignin	aliphatic OH (mmol/g)[a]	phenols (mmol/g)[a]	−COOH (mmol/g)[a]	M_n[b]	M_w[b]	PD[b]	yield (%)[c]
L-pristine	2.0	4.7	0.5	3500	8000	2.3	-
L-EtOAc	1.0	5.7	0.7	340	800	2.3	7.8
L-EtOH	1.4	5.2	0.6	780	1800	2.3	33.3
L-MeOH	1.7	5.2	0.5	1100	2500	2.2	12.7
L-acetone	1.5	4.8	0.4	1900	3800	2.0	10.4
L-residual	2.2	4.0	0.4	6900	24,000	3.5	32.6

[a]Quantified by ^{31}P NMR. [b]Determined by size exclusion chromatography (SEC) using a SEC 1260 infinity (Polymer standard service, Germany) equipped with a PSS precolumn, PSS column 100 Å, and PSS GRAM 10,000 Å analytical columns thermostated at 60 °C; the calibration plot was constructed with pullulan standards. [c]Isolated yield.

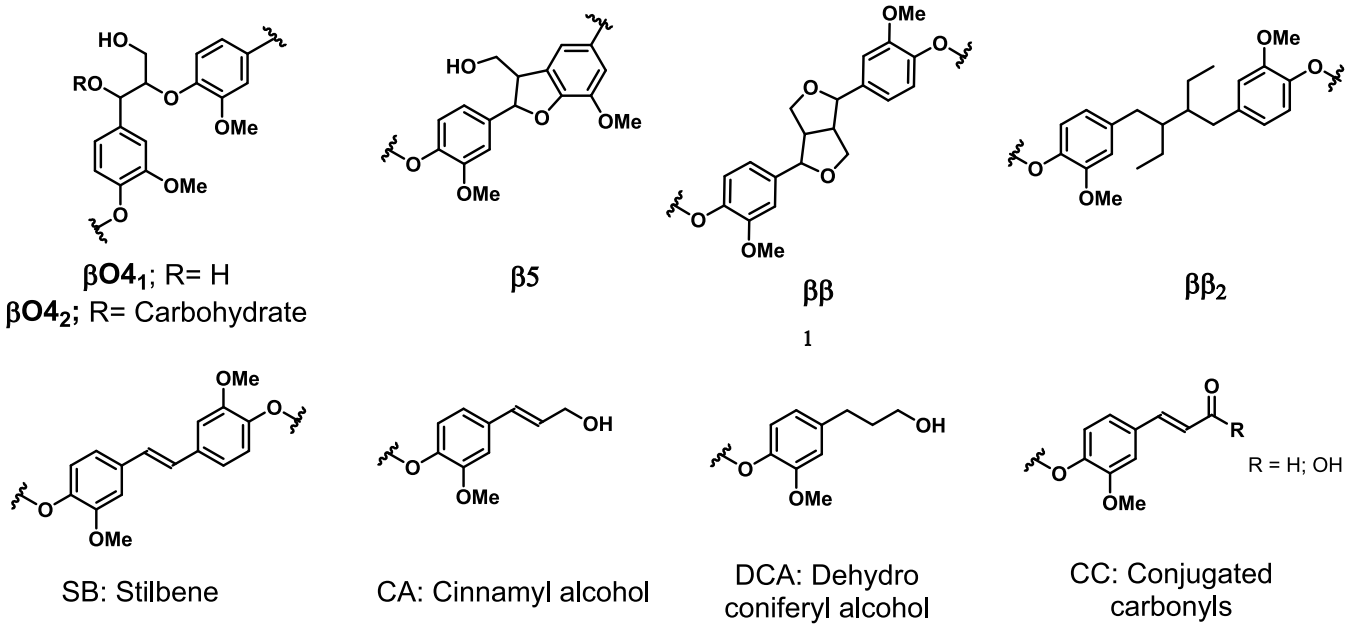

Figure 2. Main connecting units in Kraft lignin.

believe that this work may open new directions in the synthetic photochemistry promoted by natural architectures. Indeed, for the first time, technical lignin structures find a new valorization pathway, by actively contributing to photochemically triggered organic transformations. The results here obtained constitute an important step toward the exploitation of cheap and green photopromoters in organic synthesis.

2. EXPERIMENTAL SECTION

2.1. Materials. All chemicals were of analytical grade and used as received unless stated otherwise. Spruce Lignoboost Kraft Lignin was gently supplied by Chalmers University (Sweden); ethyl acetate (EtOAc), ethanol absolute (EtOH), acetone, and acetonitrile were supplied by Merk and used as received.

2.2. Lignin Fractionation. 50 g of pristine lignin (**L**-Pristine) was introduced in a flat bottom flask equipped with magnetic stirring along with 500 mL of solvent. The mixture was stirred at room temperature for 2 h; then, the soluble and insoluble fractions were separated by using a Buchner funnel with filter paper under reduced pressure. After filtration, the insoluble fraction was dried and resuspended in another solvent (in the solvent order EtOAc, EtOH, MeOH, and acetone). The soluble fraction was concentrated under reduced pressure. The lignin fractions were named based on the specific solvent used for fractionation, namely, **L**-EtOAc, **L**-EtOH, **L**-MeOH, **L**-Acetone, and **L**-Residual.

2.3. NMR Analysis. ^{1}H-, ^{13}C-, ^{19}F-NMR were recorded on a Bruker 400 Avance III HD equipped with a BBI-z grad probe head 5 mm (^{1}H: 400 MHz, ^{13}C: 100.5 MHz, ^{19}F: 376 MHz). The chemical shifts (δ) for ^{1}H and ^{13}C are given in ppm relative to residual signals of the solvents ($CHCl_3$ @7.26 ppm for ^{1}H NMR, and @77.16 ppm for ^{13}C NMR, $CFCl_3$ @0.0 ppm for ^{19}F NMR spectra). Coupling constants are given in Hz. The following abbreviations are used to indicate the multiplicity: s, singlet; d, doublet; t, triplet; q, quartet; m, multiplet; br, broad signal. NMR yields were calculated using trichloroethylene as an internal standard. ^{31}P NMR analysis was performed on a Bruker Biospin Avance spectrometer equipped with a Broadband Inverse probe and operating at a proton frequency of 400.13 MHz. Data were processed with MestreNova (Mestrelab Research) using a 90° shifted square sine-bell apodization window; baseline and phase correction were applied in both directions. The chemical shifts (δ) for ^{31}P are given in ppm relative to residual signals of the internal standard (Endo-*N*-Hydroxy-5-norbornene-2,3-dicarboximide) after phosphorylation at 151.2 ppm. The HSQC analysis of lignin fractions were performed on a Bruker Avance Neo 600 (base frequency 600 MHz for 1H nuclei) spectrometer, equipped with a broadband Z-gradient probe.

2.4. Size Exclusion Chromatography. Size exclusion chromatography (SEC), using a SEC 1260 infinity (Polymer standard service, Germany) equipped with a PSS precolumn, PSS column 100 Å, and PSS GRAM 10 000 Å analytical columns thermostated at 60 °C, was performed to determine the molecular weight and dispersity of the different lignin samples. The detection system included a UV detector in series with a refractive index detector. DMSO + 0.5% LiBr was used as an eluent with a constant flow rate of 0.5 mL/min. A calibration plot was constructed with pullulan standards. The samples were produced by solubilizing lignin in the elution mixture at a

https://doi.org/10.1021/acssuschemeng.5c05307
ACS Sustainable Chem. Eng. 2025, 13, 12300−12310

Table 2. Optimization of the Photochemical Atom Transfer Radical Addition (ATRA) Process and Control Experiments: Selected Results

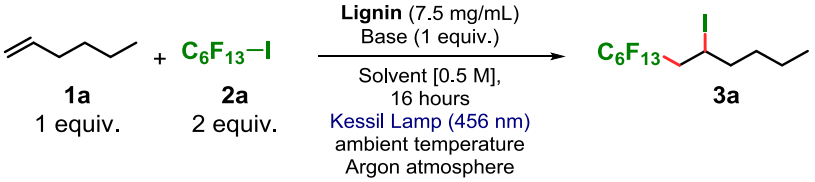

entry[a]	lignin	base	solvent	yield **3a** (%)[b]
1	L-EtOAc	2,6-lutidine	MeCN	87 (73)[c]
2[d]	L-EtOAc	2,6-lutidine	MeCN	0
3[e]	L-EtOAc	2,6-lutidine	MeCN	0
4	-	2,6-lutidine	MeCN	0
5	L-EtOAc	-	MeCN	0
6	L-Pristine	2,6-lutidine	MeCN	50
7	L-EtOH	2,6-lutidine	MeCN	61
8	L-MeOH	2,6-lutidine	MeCN	74
9	L-Acetone	2,6-lutidine	MeCN	83
10	L-Residual	2,6-lutidine	MeCN	0
11	L-EtOAc	2,6-lutidine	DMF	12
12	L-EtOAc	2,6-lutidine	EtOAc	0
13	L-EtOAc	2,6-lutidine	DCM	0
14	L-EtOAc	TMG	MeCN	0
15	L-EtOAc	DBU	MeCN	0
16	L-EtOAc	Cs_2CO_3	MeCN	<5
17	L-EtOAc	K_3PO_4	MeCN	0

[a]Reactions performed on a 0.1 mmol scale. [b]Yields were determined by ^{1}H NMR analyses on the reaction crude, using trichloroethylene as an internal standard. [c]Isolated yield. [d]Reaction performed under air or in the presence of TEMPO (2,2,6,6-tetramethylpiperidine 1-oxyl, 1 equiv). [e]Reaction performed in the dark. TMG: 1,1,3,3-tetramethylguanidine; DBU: 1,8-diazabicyclo[5.4.0]undec-7-ene. MeCN: acetonitrile; DMF: *N*,*N*-dimethylformamide; EtOAc: ethyl acetate; DCM: dichloromethane.

Scheme 1. Scope of Alkenes 1 and the Radical Precursors 2 That Can Participate in the ATRA Process. d.r.: Diastereomeric Ratio

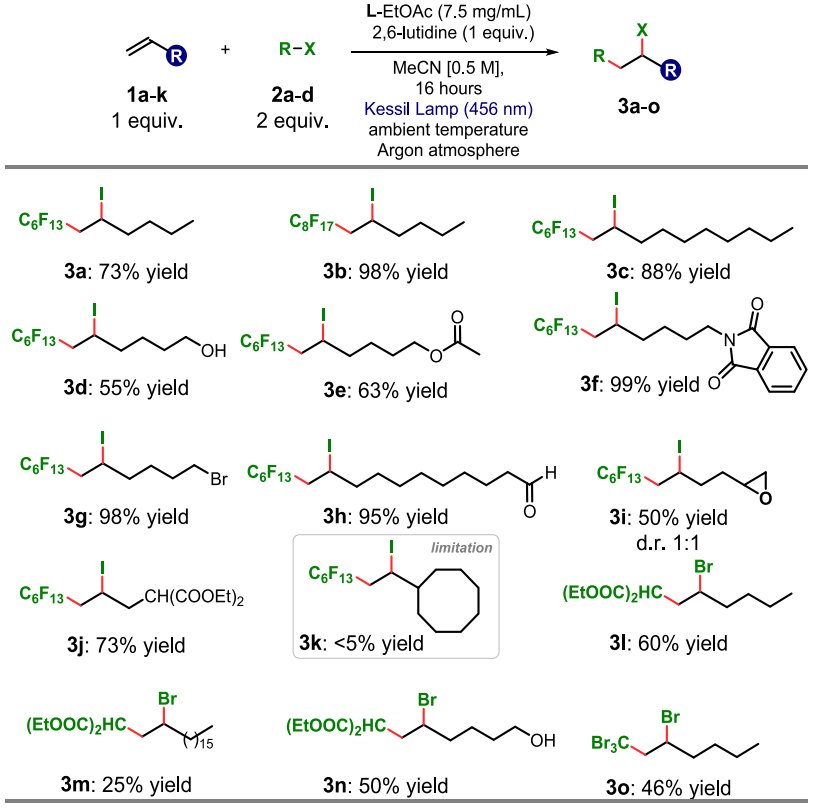

https://doi.org/10.1021/acssuschemeng.5c05307
ACS Sustainable Chem. Eng. 2025, 13, 12300−12310

concentration of 0.1 mg/mL. The mixtures were first sonicated at room temperature for 30 min and then filtered with 0.22 μm filters.

2.5. UV−Vis Spectroscopy. Absorption spectroscopy studies were performed on a Varian Cary 50 UV−vis double beam spectrophotometer. All of the spectra were recorded at room temperature using 10 mm path-length Hellma Analytics quartz cuvettes.

2.6. General Procedure for the Photochemical ATRA Reactions. A 10 mL Schlenk tube was charged with the radical precursor **2a-d** (0.2 mmol, 2.0 equiv), olefins **1a-k** (0.1 mmol, 1.0 equiv), 2,6-lutidine (0.1 mmol, 1.0 equiv), **L**-EtOAc (3 mg) and MeCN (400 μL, 0.25M). The reaction mixture was thoroughly degassed via 3 cycles of freeze−pump−thaw, and then the vessel was refilled with argon and placed at 4−5 cm from a Kessil lamp (λ = 456 nm). The temperature was kept at around 30 °C by using a fan. Stirring was maintained for 16 h. The reaction mixture was filtered over a silica plug and eluted with a mixture of hexane and ethyl acetate (95:5). The volatiles were removed in vacuo and the residue was purified by column chromatography (cyclohexane/EtOAc) to give the desired products **3a-o**.

3. RESULTS AND DISCUSSION

3.1. Lignin Refining and Characterization. Technical lignin, derived from industrial extraction processes, is mainly constituted by a heterogeneous mixture of lignin macromolecules characterized by a wide range of molecular weights and functionalities. As previously reported,[67,68] Spruce Lignoboost Kraft lignin (**L**-Pristine) was refined by exploiting the solvent solubility differences in organic solvents of lignin architectures according to their functionality and molecular weight. The method was optimized to obtain fractions presenting a range of reproducible molecular weights and a more homogeneous range of functional groups, thus striving to overcome the structural differences of technical isolated lignin resulting from variable industrial parameters, such as temperature, reaction times, and concentration. As reported in Figure 1a, the pristine lignin (**L**-Pristine) was subjected to a sequential extraction in cheap and safe organic solvents such as ethyl acetate, ethanol, methanol, and acetone. Four solvent-soluble fractions, namely, **L**-EtOAc, **L**-EtOH, **L**-MeOH, **L**-Acetone, and one residual fraction (**L**-Residual), were obtained by simple filtration and solvent evaporation. With a total yield of 96.8%, **L**-EtOH and **L**-Residual represent the most relevant fractions (Figure 1b and Table 1), while the others can be isolated in a range between 8 and 13%.

As reported in Figure 1c and Table 1, the extraction set is conceived to isolate fractions presenting an increasing average molecular weight at each extraction step. Starting from pristine lignin presenting a M_w of 8000 Da, a portfolio of fractions

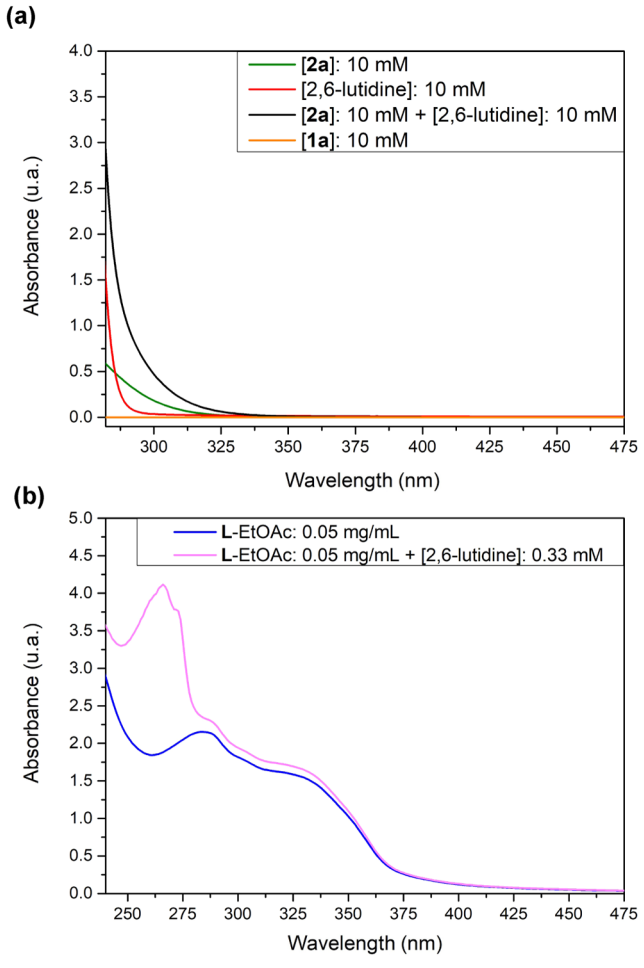

Figure 3. (a) Optical absorption spectra recorded in MeCN of **2a**, 2,6-lutidine, **1a** and a mixture of **2a** and 2,6-lutidine. (b) Optical absorption in MeCN of **L**-EtOAc and a mixture of **L**-EtOAc and 2,6-lutidine.

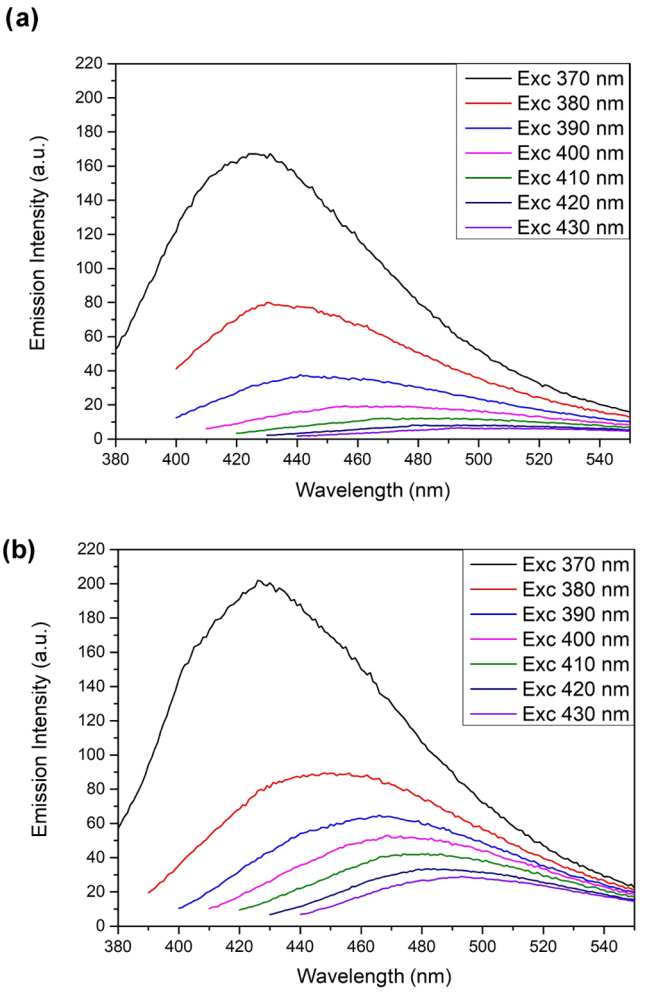

Figure 4. (a) **L**-EtOAc (0.0125 mg/mL) emission in acetonitrile. The excitation wavelengths are shown in the corresponding box. (b) **L**-EtOAc emission (0.0125 mg/mL) in the presence of 2,6-lutidine in acetonitrile ([2,6-lutidine]: 0.832 mM). The excitation wavelengths are shown in the box.

https://doi.org/10.1021/acssuschemeng.5c05307
ACS Sustainable Chem. Eng. 2025, 13, 12300−12310

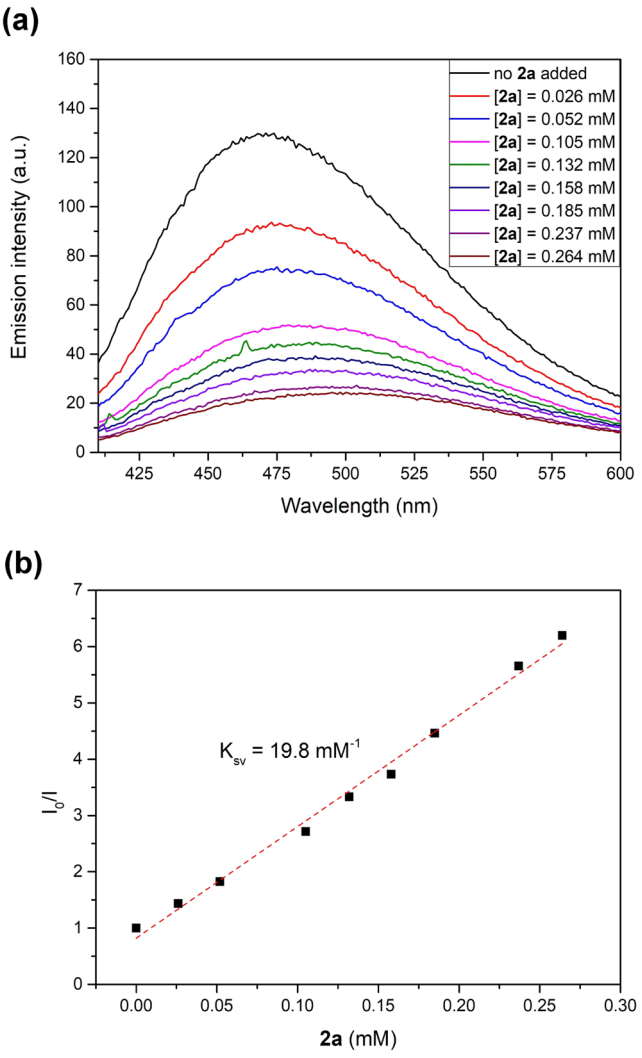

Figure 5. (a) Quenching of **L**-EtOAc emission (0.125 mg/mL, excitation at 400 nm) in the presence of 2,6-lutidine ([2,6-lutidine]: 0.005 M) and increasing amounts of **2a** in acetonitrile. (b) Linear correlation between the emission intensity (456 nm) and the concentration of **2a** in the presence of 2,6-lutidine ([2,6-lutidine]: 0.005 M).

ranging from **L**-EtOAc, constituted mainly of oligomers with a M_w of about 800 Da, up to 24,000 Da for **L**-Residual was achieved. The obtained lignin fractions were characterized by a combined 2D-heteronuclear single quantum coherence (HSQC) and ^{31}P nuclear magnetic resonance (NMR) analysis to assess and quantify the most recurring structures and functionalities. ^{31}P NMR allows, after proper functionalization, quantification of the predominant functional groups in lignin, such as phenols, aliphatic alcohols, and carboxylic acids, while 2D-HSQC analysis provides a comprehensive overview of the primary connecting units and functionalities present in the lignin backbone.

As shown in Table 1 and Figures S1–S7, ^{31}P NMR analysis demonstrated that low molecular weight fractions such as **L**-EtOAc and **L**-EtOH present a higher content of phenols and carboxylic acids while maintaining the lowest amount of aliphatic alcohols. Such fractions are the result of a more severe degradation of lignin architectures during isolation, resulting in an enhanced oxidation of the alcohols.

The HSQC spectrum of **L**-Pristine presents structures typical of softwood Kraft lignin (Figure S8). The most relevant units are represented by $\beta5$ (86.9/5.40 ppm), $\beta\beta_1$ (85.1/4.61 ppm, 53.5/3.04 ppm, and 71.1/3.81–4.15), $\beta\beta_2$ (33.5/2.42–2.53 and 42.8/1.86), and stilbene units (129.0/7.30–6.96 ppm), while the βO4 (59.4/3.42–3.71 ppm, 71.4/4.71 ppm, and 83.5/4.27 ppm), more typical of native lignin, appears substantially reduced (Figure 2). Aliphatic alcoholic end-groups such as cinnamyl alcohol (CA) and dihydro coniferyl (DCA) alcohol are detected respectively at 120.9/5.34 ppm for the former, while at 31.1/2.48 and 34.4/1.66 ppm for the latter. Conjugated carbonyls and acids can be detected at 124.0/7.78–7.45 ppm. Finally, the region related to aliphatic side chains is detectable at 30–10/2.5–0.5 ppm, while unsaturated moieties appear at 130–115/57–5.2 ppm. The isolated lignin fractions reported in Figures S9–S13 depict substantial differences concerning the main connecting units reported in Figure 2. **L**-EtOAc and **L**-EtOH (Figures S9–S10) show a complete lack of $\beta5$ units and a substantial decrease in the βO4 and stilbene units. In both fractions, carbohydrate signals (3.0–3.5/73–78 ppm) are absent, while for **L**-EtOH, the aromatic region appears less variable with a decrease of unsaturated oxidized moieties. **L**-MeOH and **L**-Acetone (Figures S11–S12) display a higher intensity for the βO4 units, while stilbene and $\beta5$ are present only marginally. Interestingly, oxidized conjugated structures, unsaturated moieties, and aliphatic side chains become irrelevant. **L**-Residual (Figure S13) indeed shows an increased intensity for βO4 while $\beta\beta$, $\beta5$, and aliphatic side chains are present only in traces. The unsaturated moieties are completely absent, while we can easily distinguish signals ascribable to carbohydrate residues.

3.2. Optimization of the Reaction Conditions. To evaluate the role of lignin as a photopromoter, an iodoperfluoroalkylation reaction between 1-hexene **1a** and perfluorohexyl iodide **2a** was performed under blue light irradiation (Kessil lamp, λ_{max} = 456 nm, lamp power: 50 W) at ambient temperature (Table 2). Specifically, the preliminary experiment was conducted using acetonitrile as the solvent, **L**-EtOAc (loading: 7.5 mg/mL), and 2,6-lutidine (1 equiv) as an organic base (entry 1, Table 2). Interestingly, under these reaction conditions, we observed the formation of the desired product **3a** in good chemical yield (87%). Afterward, a series of control experiments was carried out to obtain more mechanistic insights on the studied transformation (entries 2–5, Table 2). In particular, no reaction occurs in the presence of TEMPO (2,2,6,6-tetramethylpiperidine 1-oxyl, 1 equiv) or air (entry 2, Table 2). These experiments are consistent with a radical mechanism. We also confirmed that the studied reaction is initiated by the photochemical activity of **L**-EtOAc. Indeed, we did not observe the formation of product **3a** neither in the dark nor in the absence of lignin (entries 3–4, Table 2). Similarly, a complete inhibition of reactivity has been observed without 2,6-lutidine (entry 5, Table 2), which is a non-nucleophilic organic base. Indeed, **L**-EtOAc shows several acidic moieties (*e.g.*, carboxylic acids) that can be easily deprotonated through the use of 2,6-lutidine (see Table 1). Then, the different fractions of lignin were tested in the model reaction (entries 6–10, Table 2). The use of the soluble fractions, namely, **L**-Pristine, **L**-MeOH, **L**-EtOH, and **L**-Acetone—provided the desired product in good chemical yields, spanning between 50 and 83%. On the other hand, the formation of **3a** was not observed when using **L**-Residual

https://doi.org/10.1021/acssuschemeng.5c05307
ACS Sustainable Chem. Eng. 2025, 13, 12300–12310

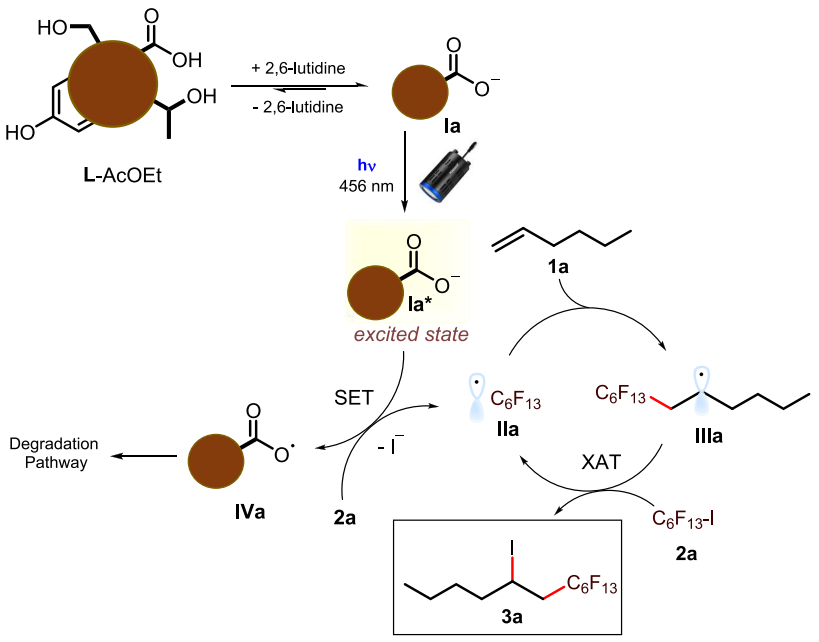

Figure 6. Proposed mechanism for the reaction for the photochemical iodofluoroalkylation of **1a** with **2a** in the presence of 2,6-lutidine. SET: single-electron transfer; XAT: halogen-atom transfer.

(entry 10, Table 2). These experiments pointed out that the solubility of the lignin fraction is a critical factor in this photochemical transformation. In this regard, atomic force microscopy (AFM) analysis was used to determine the dimensions of **L**-EtOAc, which turned out to be 3.2 ± 1.4 nm (Figure S16). Based on available data, this fraction appears to be mainly composed of small oligomers and nanometric particles (M_w = 800 Da, see Table 1), which shows high solubility in acetonitrile and more generally in polar organic solvents. Then, different solvents were tested for the model reaction (entries 11−13, Table 2), such as dimethylformamide (DMF), ethyl acetate (EtOAc), and dichloromethane (DCM). Unfortunately, none of these solvents could rival the performance offered by acetonitrile (MeCN). Further screening of the bases did not bring any improvement in the efficiency of the model reaction (entries 14−17, Table 2). In particular, we observed that the use of strong organic bases (such as TMG: 1,1,3,3-tetramethylguanidine and DBU: 1,8-diazabicyclo[5.4.0]undec-7-ene), which may deprotonate also the less acidic moieties of **L**-EtOAc (*e.g.*, phenols), led to the precipitation of the lignin forming an insoluble material under the reaction conditions. As a matter of fact, the presence of solid particles may reduce the amount of the photoactive material in solution, while also leading to the scattering of the irradiating light. These two aspects have possibly precluded effective initiation of the radical reaction. Since **L**-EtOAc resulted in the best-performing fraction, a structural assessment after being recovered from the reaction mixture was performed by ^{31}P NMR and HSQC. As shown in Figure S7, a loss of 98% of the aliphatic alcohols, 95% of the phenols, and 94% of the carboxylic acids, respectively, was detected in the recovered lignin. These results suggest that **L**-EtOAc underwent extensive decarboxylation and dehydration reactions in the photochemical regime. Also, the main structure of lignin was affected (Figure S14) with a substantial reduction of βO4 and $\beta\beta$, while β5, stilbene units, and unsaturated moieties were completely absent. In addition, the spectra reported an increase of conjugated oxidized moieties in the range 7.75−7.65 ppm along with a qualitative depletion of the secondary carbons in the aliphatic region (2.75−1.00 ppm).

Finally, size exclusion chromatography (SEC) shows that postreaction **L**-EtOAc presents a wider polydispersity and the appearance of lignin fragments at higher retention times (Figure S17). Indeed, lignin is involved in concomitant structural modifications under the reaction conditions, on the one hand by partially producing lower M_w fragments and on the other by being subjected to grafting processes of fluorinated moieties on the structure (Figure S15) with concomitant consumption of the main functional groups. Indeed, we observed that some fluorinated radicals may react with lignin's functionalities, most probably with the aromatic groups and olefins. We also studied the stability of a solution of **L**-EtOAc in MeCN when irradiated with a Kessil lamp at 456 nm over 16 h (under an argon atmosphere). In particular, the material proved to be stable under these operative conditions, as its chemical structure was not degraded under blue light irradiation. This result further suggested that the degradation of the material mainly took place under the reaction conditions when in the presence of the starting materials/additives. Using the optimized reaction conditions (entry 1, Table 2), we demonstrated the generality of the photochemical reaction (Scheme 1). In addition to the perfluorohexyl chain (product **3a**), a longer perfluorinated substituent was installed with an excellent yield to give **3b**. We also demonstrated that the reaction efficiently tolerates various terminal olefins **1** containing alkyl chains, alcohol, ester, imide, halide, aldehyde, and epoxide moieties (products **3c**-**j**). Surprisingly, the use of olefin **1j** did not afford the desired product (**3k**). In this regard, we believe that the poor reactivity of this alkene is due to its increased steric hindrance. This aspect may prevent this olefin from effectively undergoing an ATRA process. In addition, an ATRA reaction between $BrCCl_3$ and 1-hexene was performed under the optimized operative conditions. In particular, we observed the formation of the final product in a low NMR yield (about 12%).

https://doi.org/10.1021/acssuschemeng.5c05307
ACS Sustainable Chem. Eng. 2025, 13, 12300−12310

Moreover, we found that styrene was not a suitable substrate for this reaction. Indeed, this reaction did not lead to the formation of the final product when this olefin was reacted with perfluorohexyl iodide. Importantly, other easily reducible alkyl halides **2** may be used as radical precursors, namely diethyl bromomalonate **2c** and tetrabromomethane **2d**. In particular, products **3l-o** were isolated in moderate to good chemical yields (up to 60%). All products (**3a-o**) were found to be stable over time when stored in a desiccator at ambient temperature. In addition, we tried to reuse the material after being recovered from a photochemical reaction. The tests demonstrated that the recycled material was not a competent photoinitiator, since it was not able to trigger a second ATRA reaction.

3.3. Mechanistic Studies. To gain further insights into the role of the **L**-EtOAc in the photochemical process, we investigated its photophysical behavior. We first recorded the absorption spectra of all of the reaction components in MeCN to make sure that **L**-EtOAc is the only species capable of absorbing light at 456 nm (Figure 3). Specifically, we observed that 1-hexene **1a** may not absorb light in the range between 300 and 500 nm (yellow line in Figure 3a). On the other hand, the perfluorohexyl iodide **2a** (green line in Figure 3a) and 2,6-lutidine (red line in Figure 3a) do absorb photons only in the UV region of the spectrum. Moreover, we observed the formation of an electron donor−acceptor (EDA) complex between **2a** and 2,6-lutidine (black line in Figure 3a). However, this aggregate does not absorb light at 456 nm. On the other hand, **L**-EtOAc can absorb light at 456 nm (Figures 3b and S18). We also measured the extinction coefficient of **L**-EtOAc at 456 nm ($\varepsilon_{456\text{L-EtOAc}}$ = 0.48 mL/cm·mg). The extinction coefficients at 456 nm have also been calculated for all soluble lignin fractions (Figures S18−24 and Table S1). Moreover, we noted a slight red shift in the absorption of **L**-EtOAc when mixed with 2,6-lutidine, along with an increase in absorbance within the range between 300 and 360 nm (Figure 3b). The deprotonation of carboxylic moieties on lignin, with concomitant formation of surface carboxylate anions, could be the cause of this behavior. Importantly, the material showed good solubility in MeCN even after the addition of the base. These results, along with the control experiments depicted in Table 2 (entries 3−5), suggested the key role played by the deprotonated material in photoinitiating the radical process.

Moreover, the fluorescence spectra of **L**-EtOAc showed a dependence between the emission maximum and the excitation wavelength (Figure 4), similarly to other organic nanostructured materials.[72,73] Interestingly, this trend became more pronounced with the addition of 2,6-lutidine. Afterward, we demonstrated that **2a** was capable of quenching the excited state of **L**-EtOAc when in the presence of 2,6-lutidine (Figure 5).

In particular, we observed a linear Stern−Volmer correlation (K_{sv} = 19.8 mM^{-1}) consistent with the occurrence of a single type of quenching phenomenon, most probably *via* a single-electron transfer (SET) mechanism (Figure 5b). Since the organic material is presumably negatively charged, it is reasonable to assume that this photoinduced process likely proceeds through a SET event. Mechanistically, we thus believe that the base could deprotonate the carboxylic acids present on **L**-EtOAc, which are the more acidic functionalities within the material, thus resulting in the formation of a soluble negatively charged material with an enhanced photoreducing capability. Then, the photoinduced oxidation of the surface carboxylate anions, executed by the interaction with **2a**, might trigger their decarboxylation, releasing CO_2 as a gas. This irreversible transformation might initiate a material degradation process. In this regard, it is well-known that, upon an oxidation step, carboxylate anions can easily undergo decarboxylation, resulting in the formation of radicals and CO_2,[74] in agreement with the previously reported HSQC and ^{31}P NMR results (Figures S7 and S14). Then, the Stern−Volmer constant was also calculated for all of the soluble lignin fractions in the presence of 2,6-lutidine. Indeed, **L**-EtOH, **L**-MeOH, and **L**-Acetone presented a K_{sv} of 19.2, 17.4, and 13.8 mM^{-1}, respectively. Interestingly, **L**-EtOAc showed the highest K_{sv} (see Table S1), which can be correlated to the highest yield obtained in the model reaction (see Table 2, entry 1). Moreover, it is worth mentioning that **L**-EtOAc showed the highest number of carboxylic acids and was the most soluble fraction in acetonitrile (see Table 1). Taken together, these aspects may tentatively explain the higher activity of **L**-EtOAc in driving the studied reaction. In light of the information at our disposal, we were able to propose a reaction mechanism (Figure 6). Upon addition to the reaction mixture, 2,6-lutidine probably deprotonates the carboxylic groups present on the surface of **L**-EtOAc, increasing its reducing power. The deprotonated species of lignin (**Ia**) absorbs light at 456 nm, reaching an electronically excited state (**Ia***). **Ia*** is then quenched by **2a**, upon an SET event. This single-electron transfer process leads to breaking of the carbon−iodine bond, thus generating the first radical (**IIa**) needed for triggering the ATRA reaction. Indeed, perfluorohexyl iodide **2a** is a well-known radical precursor that can be easily reduced (E_{red} = −1 V vs SCE) to yield a fluorinated alkyl radical and I^- as a leaving group.[75] After the photochemical initiation step, radical **IIa** is intercepted by olefin **1a**, yielding intermediate **IIIa**. At last, a halogen-atom transfer (XAT) occurs that generates the final product **3a** and regenerates **IIa**. On the other hand, the oxidized lignin (**IVa**) may undergo radical degradation pathways that drastically alter the chemical structure of the material, while reducing the number of oxygenated functionalities.

4. CONCLUSIONS

To conclude, we demonstrated for the first time the possibility of effectively exploiting low molecular weight refined lignin as a photochemical initiator for relevant ATRA reactions. Indeed, the molecular weight and the presence of carboxylic acid moieties resulted as pivotal structural features in promoting the reaction. The mechanistic studies suggested that the lignin carboxylate intermediate produced *in situ* upon deprotonation of the acidic moieties by 2,6-lutidine is the main factor responsible for photoreduction of the radical fluorinated precursors. As a result, this method allowed the production of several alkyl halides from moderate to excellent yields and under mild operating conditions. Importantly, **L**-EtOAc proved to be an extremely competent photoinitiator. Indeed, we used this material with a very low loading (0.2 mol %, calculated on the basis of M_w = 800 Da) to synthesize the desired model product **3a** with a good level of productivity, namely 3 $mmol_{3a}$ h^{-1} $g_{L\text{-EtOAc}}{}^{-1}$. In this context, classical organic photoinitiators include hydroxy ketones, phosphine oxides, benzophenones, thioxanthones, among others. It is important to highlight that the use of **L**-EtOAc shows advantages over that of classical photoactive molecular

https://doi.org/10.1021/acssuschemeng.5c05307
ACS Sustainable Chem. Eng. 2025, 13, 12300−12310

initiators. In particular, **L**-EtOAc is inexpensive, nontoxic, and readily available on a large scale. Moreover, it is worth mentioning that classical radical (photo)initiators are generally used in stochiometric or substochiometric amounts (up to 100 mol %). Importantly, this photochemical approach allowed the synthesis of relevant fluorinated compounds that have been widely used in numerous fields of application including medicinal chemistry, agrochemistry, and materials science. These considerations highlighted a brand-new role for a heterogeneous recalcitrant byproduct such as lignin. Indeed, this work introduces a novel valorization approach for lignin, laying the basis for exploring future sustainable photochemical processes promoted by well-defined biobased compounds. Therefore, we expect that future investigations in such research area will contribute to determine new directions in organic synthesis for both academia and industry.

■ ASSOCIATED CONTENT

Supporting Information

The Supporting Information is available free of charge at https://pubs.acs.org/doi/10.1021/acssuschemeng.5c05307.

Experimental procedures, material characterization, NMR spectra, chromatograms, and the characterization for all organic compounds (PDF)

■ AUTHOR INFORMATION

Corresponding Authors

Claudio Gioia − *Department of Physics, University of Trento, Trento 38123, Italy*; Email: claudio.gioia@unitn.it

Giacomo Filippini − *Department of Chemical and Pharmaceutical Sciences, INSTM UdR Trieste, University of Trieste, 34127 Trieste, Italy*; orcid.org/0000-0002-9694-3163; Email: gfilippini@units.it

Authors

Vasco Corti − *Department of Chemical and Pharmaceutical Sciences, INSTM UdR Trieste, University of Trieste, 34127 Trieste, Italy*

Alessandro Filippini − *Phenbiox SRL, 40123 Bologna, Italy*

Dario Zanichelli − *Phenbiox SRL, 40123 Bologna, Italy*

Francesco Palazzi − *Department of Chemical and Pharmaceutical Sciences, INSTM UdR Trieste, University of Trieste, 34127 Trieste, Italy*

Pavel Solovyev − *Research and Innovation Centre, Edmund Mach Foundation, 38098 San Michele all'Adige, TN, Italy*; orcid.org/0000-0001-7152-3157

Maurizio Prato − *Department of Chemical and Pharmaceutical Sciences, INSTM UdR Trieste, University of Trieste, 34127 Trieste, Italy; Centre for Cooperative Research in Biomaterials (CIC BiomaGUNE), Basque Research and Technology Alliance (BRTA), 20014 Donostia-San Sebastián, Spain; Basque Foundation for Science Ikerbasque, 48013 Bilbao, Spain*; orcid.org/0000-0002-8869-8612

Complete contact information is available at: https://pubs.acs.org/10.1021/acssuschemeng.5c05307

Author Contributions

The manuscript was written through contributions of all authors. All authors have given approval to the final version of the manuscript.

Notes

The authors declare no competing financial interest.

■ ACKNOWLEDGMENTS

G.F. kindly acknowledges FRA2024 funded by the University of Trieste and Microgrants 2024 funded by Region FVG. C.G. kindly acknowledges Giada Lo Re's group (Chalmers university of Technology) for their precious know-how on lignin. P.S. kindly acknowledges FRUITOMICS FESR 2014-2020 program funded by the Autonomous Province of Trento

■ REFERENCES

(1) Pintauer, T.; Matyjaszewski, K. Organometallic-Mediated Radical Polymerization. In *Encyclopedia of Radicals*; Wiley: Hoboken, 2012; Vol. 4, pp 1851−1894.

(2) Bag, D.; Kour, H.; Sawant, S. D. Recent advances in organocatalytic C−H functionalization. *Org. Biomol. Chem.* **2020**, *18*, 8278−8293.

(3) Curran, D. P.; Bosch, E.; Kaplan, J.; Newcomb, M. Rate Constants for Halogen Atom Transfer from Representative α-Halo Carbonyl Compounds to Primary Alkyl Radicals. *J. Org. Chem.* **1989**, *54*, 1826−1831.

(4) Curran, D. P.; Chen, M.-H.; Spletzer, E.; Seong, C. M.; Chang, C.-T. Atom-Transfer Addition and Annulation Reactions of Iodomalonates. *J. Am. Chem. Soc.* **1989**, *111*, 8872−8878.

(5) Curran, D. P.; Seong, C. M. Atom Transfer Addition, Annulation, and Macrocyclization Reactions of Iodomalononitriles. *J. Am. Chem. Soc.* **1990**, *112*, 9401−9403.

(6) Curran, D. P.; Tamine, J. Effects of Temperature on Atom Transfer Cyclization Reactions of Allylic Iodides. *J. Org. Chem.* **1991**, *56*, 2746−2750.

(7) Yorimitsu, H.; Nakamura, T.; Shinokubo, H.; Oshima, K. Triethylborane-Mediated Atom Transfer Radical Cyclization Reaction in Water. *J. Org. Chem.* **1998**, *63*, 8604−8605.

(8) Yorimitsu, H.; Nakamura, T.; Shinokubo, H.; Oshima, K.; Omoto, K.; Fujimoto, H. Powerful Solvent Effect of Water in Radical Reaction: Triethylborane-Induced Atom-Transfer Radical Cyclization in Water. *J. Am. Chem. Soc.* **2000**, *122*, 11041−11047.

(9) Yorimitsu, H.; Shinokubo, H.; Matsubara, S.; Oshima, K. Triethylborane-Induced Atom-Transfer Radical Cyclization in Water. *J. Org. Chem.* **2001**, *66*, 7776−7785.

(10) Baciocchi, E.; Muraglia, E. Synthesis of γ-Haloesters and γ-Ketoesters by Homolytic Addition of Carbon Radicals Generated by α-Haloesters and Triethylborane to Alkenes and Silyl Enol Ethers. *Tetrahedron Lett.* **1994**, *35*, 2763−2766.

(11) Renaud, P.; Ollivier, C.; Panchaud, P. Radical Carboazidation of Alkenes: An Efficient Tool for the Preparation of Pyrrolidinone Derivatives. *Angew. Chem., Int. Ed.* **2002**, *41*, 3460−3462; *Angew. Chem.* **2002**, *114*, 3610−3612.

(12) (a) Panchaud, P.; Ollivier, C.; Renaud, P.; Zigmantas, S. Radical Carboazidation: Expedient Assembly of the Core Structure of Pyrrolidinone Derivatives. *J. Org. Chem.* **2004**, *69*, 2755−2759. (b) Weidner, K.; Giroult, A.; Panchaud, P.; Renaud, P. Efficient Carboazidation of Alkenes Using a Radical Desulfonylative Azide Transfer Process. *J. Am. Chem. Soc.* **2010**, *132*, 17511−17515.

(13) Kharasch, M. S.; Jensen, E. V.; Urry, W. H. Addition of Carbon Tetrachloride and Chloroform to Olefins. *Science* **1945**, *102* (2640), No. 128.

(14) Kharasch, M. S.; Skell, P. S.; Fisher, P. Reactions of Atoms and Free Radicals in Solution. XII. The Addition of Bromo Esters to Olefins. *J. Am. Chem. Soc.* **1948**, *70*, 1055−1059.

(15) Dolbier, W. R., Jr. Structure, Reactivity, and Chemistry of Fluoroalkyl Radicals. *Chem. Rev.* **1996**, *96*, 1557−1584.

(16) Brace, N. O. Syntheses with perfluoroalkyl radicals from perfluoroalkyl iodides. A rapid survey of synthetic possibilities with emphasis on practical applications. Part one: alkenes, alkynes and allylic compounds. *J. Fluorine Chem.* **1999**, *93*, 1−25.

(17) Nikitas, N. F.; Voutyritsa, E.; Gkizis, P. L.; Kokotos, C. G. Metal-Free Photochemical Atom Transfer Radical Addition (ATRA) of $BrCCl_3$ to Alkenes. *Eur. J. Org. Chem.* **2021**, *2021*, 96−101.

(18) Engl, S.; Reiser, O. Copper-Photocatalyzed ATRA Reactions: Concepts, Applications, and Opportunities. *Chem. Soc. Rev.* **2022**, *51*, 5287−5299.
(19) Wallentin, C.-J.; Nguyen, J. D.; Finkbeiner, P.; Stephenson, C. R. J. Visible Light-mediated Atom Transfer Radical Addition via Oxidative and Reductive Quenching of Photocatalysts. *J. Am. Chem. Soc.* **2012**, *134*, 8875−8884.
(20) Arceo, E.; Montroni, E.; Melchiorre, P. Photo-Organocatalysis of Atom-Transfer Radical Additions to Alkenes. *Angew. Chem., Int. Ed.* **2014**, *53*, 12064−12068.
(21) Filippini, G.; Silvi, M.; Melchiorre, P. Enantioselective Formal α-Methylation and α-Benzylation of Aldehydes by Means of Photo-Organocatalysis. *Angew. Chem., Int. Ed.* **2017**, *56*, 4447−4451.
(22) Magagnano, G.; Gualandi, A.; Marchini, M.; Mengozzi, L.; Ceroni, P.; Cozzi, P. G. Photocatalytic ATRA Reaction Promoted by Iodo-Bodipy and Sodium Ascorbate. *Chem. Commun.* **2017**, *53*, 1591−1594.
(23) Rawner, T.; Lutsker, E.; Kaiser, C. A.; Reiser, O. Enabling Photoredox-Mediated Radical [^{18}F]Trifluoromethylation Using a Heteroleptic Copper-Based Photocatalyst. *ACS Catal.* **2018**, *8*, 3950−3956.
(24) Mei, T.-S.; Zhang, L.-P.; Li, Y.-Q.; Zhang, K.; Fang, P.; et al. Transition-Metal-Catalyzed Carboxylation of Organic Halides and Their Surrogates with Carbon Dioxide. *Synthesis* **2018**, *50*, 35−48.
(25) Voutyritsa, E.; Kokotos, C. G.; Triandafillidi, I.; Hatzidimitriou, A. G. Expanding the Scope of Photocatalysis: Atom Transfer Radical Addition of Bromoacetonitrile to Aliphatic Olefins. *ChemCatChem* **2018**, *10*, 2466−2470.
(26) Kokotos, C. G.; Triandafillidi, I.; Tzouras, N. V.; et al. Photocatalytic Atom Transfer Radical Addition to Olefins Utilizing Novel Photocatalysts. *Molecules* **2019**, *24*, No. 1644.
(27) Rosso, C.; Filippini, G.; Cozzi, P. G.; Gualandi, A.; Prato, M. Highly Performing Iodoperfluoroalkylation of Alkenes Triggered by the Rational Design of Reducing Organophotoredox Catalysts. *ChemPhotoChem* **2019**, *3*, 193−197.
(28) Cordero-Vargas, A.; Stevens, E. D.; Stephenson, C. R. J. Photoredox-Catalyzed Atom Transfer Radical Addition to Enals and Enones: Divergent Pathways for Alkyl Radical Addition and Reductive Dehalogenation. *Org. Lett.* **2019**, *21*, 4092−4096.
(29) Xu, F.; Zhang, Y.; Chen, G.; Wang, S. Visible-Light Photoredox Catalysis for Atom Transfer Radical Addition (ATRA) Reaction. *Chem. Commun.* **2020**, *56*, 2206−2209.
(30) Reiser, O. Visible-Light-Induced Transition-Metal Photocatalysis: Organic Synthesis and Beyond. *ACS Catal.* **2020**, *10*, 9899−9906.
(31) Miura, T.; Hoshi, Y.; Usami, S.; Sekiguchi, K. Visible-Light-Mediated Difunctionalization of Alkenes Using a Photocatalyst with Radical-Generating Ability. *Org. Biomol. Chem.* **2023**, *21*, 8642−8645.
(32) Kokotos, C. G.; Onidas, D. P. Photochemical Synthesis of Lactones, Cyclopropanes and ATRA Products: Revealing the Role of Sodium Ascorbate. *Chem. - Eur. J.* **2024**, *30*, No. e202400253.
(33) Mao, L.-L.; Cong, H. Atom Transfer Radical Addition to Unactivated Alkenes Employing Heterogeneous Visible Light Photocatalysis. *ChemSusChem* **2017**, *10*, 4461−4464.
(34) Rosso, C.; Filippini, G.; Prato, M. Use of Nitrogen-Doped Carbon Nanodots for the Photocatalytic Fluoroalkylation of Organic Compounds. *Chem. - Eur. J.* **2019**, *25*, 16032−16036.
(35) Filippini, G.; Longobardo, F.; Forster, L.; Criado, A.; Di Carmine, G.; Nasi, L.; D'Agostino, C.; Melchionna, M.; Fornasiero, P.; Prato, M. Light-Driven, Heterogeneous Organocatalysts for C−C Bond Formation Toward Valuable Perfluoroalkylated Intermediates. *Sci. Adv.* **2020**, *6*, No. eabc9923.
(36) Longobardo, F.; Gentile, G.; Criado, A.; Actis, A.; Colussi, S.; Dal Santo, V.; Chiesa, M.; Filippini, G.; Fornasiero, P.; Prato, M.; Melchionna, M. Singlet−Triplet Energy Inversion in Carbon Nitride Photocatalysts. *Mater. Chem. Front.* **2021**, *5*, 7267−7275.
(37) Rosso, C.; Cuadros, S.; Barison, G.; Costa, P.; Kurbasic, M.; Bonchio, M.; Prato, M.; Dell'Amico, L.; Filippini, G. Unveiling the Synthetic Potential of Substituted Phenols as Fully Recyclable Organophotoredox Catalysts for the Iodosulfonylation of Olefins. *ACS Catal.* **2022**, *12*, 4290−4295.
(38) Lama, A. D.; Bartolomei, B.; Rosso, C.; Filippini, G.; Martínez, M. M.; Sarandeses, L. A.; Prato, M. New Insights into the Exploitation of BODIPY Derivatives as Organic Photocatalysts. *Eur. J. Org. Chem.* **2022**, *2022*, No. e202200622.
(39) König, B. Photocatalysis in Organic Synthesis − Past, Present, and Future. *Eur. J. Org. Chem.* **2017**, *2017*, 1979−1981.
(40) Cao, L.; Yu, I. K. M.; Liu, Y.; Ruan, X.; Tsang, D. C. W.; Hunt, A. J.; Oke, Y. S.; Song, H.; Zhang, S. Lignin Valorization of food supply chain wastes into value-added chemicals: State-of-the-art review and future prospects. *Bioresour. Technol.* **2018**, *269*, 465−475.
(41) Bajwa, D. S.; Pourhashem, G.; Ullah, A. H.; Bajwa, S. G. A concise review of current lignin production, applications, products and their environmental impact. *Ind. Crops Prod.* **2019**, *139*, No. 111526.
(42) Dessbesell, L.; Paleologou, M.; Leitch, M.; Pulkki, R.; Xu, C. C. Global lignin supply overview and kraft lignin potential as an alternative for petroleum-based polymers. *Renewable Sustainable Energy Rev.* **2020**, *123*, No. 109768.
(43) Liu, Q.; Luo, L.; Zheng, L. Lignins: Biosynthesis and Biological Functions in Plants. *Int. J. Mol. Sci.* **2018**, *19*, No. 335.
(44) Zhao, Q. Lignification: Flexibility, Biosynthesis and Regulation. *Trends Plant Sci.* **2016**, *21*, 713−721.
(45) Albinsson, B.; Li, S.; Lundquist, K.; Stomberg, R. The origin of lignin fluorescence. *J. Mol. Struct.* **1999**, *508*, 19−27.
(46) Radotić, K.; Kalauzi, A.; Djikanović, D.; Jeremić, M.; LeBlanc, R. M.; Cerović, Z. G. Component analysis of the fluorescence spectra of a lignin model compound. *J. Photochem. Photobiol., B* **2006**, *83*, 1−10.
(47) Xue, Y.; Qiu, X.; Wu, Y.; Qian, Y.; Zhou, M.; Deng, Y.; Li, Y. Aggregation-induced emission: The origin of lignin fluorescence. *Polym. Chem.* **2016**, *7*, 3502−3508.
(48) Xue, Y.; Qiu, X.; Ouyang, X. Insights into the effect of aggregation on lignin fluorescence and its application for microstructure analysis. *Int. J. Biol. Macromol.* **2020**, *154*, 981−988.
(49) Xue, Y.; Wan, Z.; Ouyang, X.; Qiu, X. Lignosulfonate: A Convenient Fluorescence Resonance Energy Transfer Platform for the Construction of a Ratiometric Fluorescence pH-Sensing Probe. *J. Agric. Food Chem.* **2019**, *67*, 1044−1051.
(50) Shen, Q.; Xue, Y.; Zhang, Y.; Li, T.; Yang, T.; Li, S. Effect of microstructure-scale features on lignin fluorescence for preparation of high fluorescence efficiency lignin-based nanomaterials. *Int. J. Biol. Macromol.* **2022**, *202*, 520−528.
(51) Ratanasumarn, N.; Chitprasert, P. Cosmetic Potential of Lignin Extracts from Alkaline-Treated Sugarcane Bagasse: Optimization of Extraction Conditions Using Response Surface Methodology. *Int. J. Biol. Macromol.* **2020**, *153*, 138−145.
(52) Wang, B.; Sun, D.; Wang, H.-M.; Yuan, T.-Q.; Sun, R.-C. Green and Facile Preparation of Regular Lignin Nanoparticles with High Yield and Their Natural Broad-Spectrum Sunscreens. *ACS Sustainable Chem. Eng.* **2019**, *7*, 2658−2666.
(53) Hynynen, J.; Riddell, A.; Achour, A.; Takacs, Z.; Wallin, M.; Parkås, J.; Bernin, D. 'Lignin and Extractives First' Conversion of Lignocellulosic Residual Streams Using UV Light from LEDs. *Green Chem.* **2021**, *23*, 8251−8259.
(54) Sadeghifar, H.; Ragauskas, A. Lignin as a UV Light Blocker—A Review. *Polymers* **2020**, *12*, No. 1134.
(55) Zhang, Y.; Naebe, M. Lignin: A Review on Structure, Properties, and Applications as a Light-Colored UV Absorber. *ACS Sustainable Chem. Eng.* **2021**, *9*, 1427−1442.
(56) Wang, D.; Gu, Y.; Feng, S.; Yang, W.; Dai, H.; Xiao, H.; Han, J. Lignin-Containing Biodegradable UV-Blocking Films: A Review. *Green Chem.* **2023**, *25*, 9020−9044.
(57) Goliszek, M.; Podkościelna, B.; Smyk, N.; Sevastyanova, O. Synthesis and Characterization of Lignin-Based Copolymers with Enhanced Thermal Stability. *Pure Appl. Chem.* **2023**, *95*, 475−486.

https://doi.org/10.1021/acssuschemeng.5c05307
ACS Sustainable Chem. Eng. 2025, 13, 12300−12310

(58) Guo, H.; Luo, X.; Wang, L.; Yang, C.; Li, S.; Liu, S.; Li, J.; Chen, Z. Lignin-Assisted Photoreactions: Unveiling New Frontiers in Light-Induced Chemistry. *ChemSusChem* **2024**, *17*, No. e202402117.
(59) Gu, L.; Liu, X.; Dong, S.; Chen, Z.; Han, R.; He, C.; Wang, D.; Zheng, Y. Natural lignin nanoparticles: a promising nano-crosslinker for constructing fluorescent photoswitchable supramolecular hydrogels. *Polym. Chem.* **2020**, *11*, 1871−1876.
(60) Wang, M.; Yin, W.-M.; Zhai, Y.; Zhou, J.; Liu, S.; Li, J.; Li, S.; James, T. D.; Chen, Z. Solvent-free processing of lignin into robust room temperature phosphorescent materials. *Nat. Commun.* **2025**, *16*, No. 2455.
(61) Barapatre, A.; Meena, A. S.; Mekala, S.; Das, A.; Jha, H. In vitro evaluation of antioxidant and cytotoxic activities of lignin fractions extracted from Acacia nilotica. *Int. J. Biol. Macromol.* **2016**, *86*, 443−453.
(62) An, L.; Wang, G.; Jia, H.; Liu, C.; Sui, W.; Si, C. Fractionation of enzymatic hydrolysis lignin by sequential extraction for enhancing antioxidant performance. *Int. J. Biol. Macromol.* **2017**, *99*, 674−681.
(63) Matos, M.; Claro, F. C.; Lima, T. A. M.; Avelino, F.; Hansel, F. A.; Maciel, G. M.; Lomonaco, D.; Magalhães, W. L. E. Acetone:Water fractionation of pyrolytic lignin improves its antioxidant and antibacterial activity. *J. Anal. Appl. Pyrolysis* **2021**, *156*, No. 105175.
(64) Cheng, X.-C.; Qin, Z.; Yang, Q.-L.; Liu, H.-M.; Wang, X.-D.; Liu, Y.-L. Structural characterization and antioxidant activity of lignin from Bambusa pervariabilis McClure. *BioResources* **2021**, *16*, 2714−2730.
(65) Tagami, A.; Gioia, C.; Lauberts, M.; Budnyak, T.; Moriana, R.; Lindström, M. E.; Sevastyanova, O. Solvent fractionation of softwood and hardwood kraft lignins for more efficient uses: Compositional, structural, thermal, antioxidant and adsorption properties. *Ind. Crops Prod.* **2019**, *129*, 123−134.
(66) Li, H.; Yuan, Z.; Xing, Y.; Li, J.; Fang, J.; Changa, L.; Li, C. Acetone fractionation: a simple and efficient method to improve the performance of lignin for dye pollutant removal. *RSC Adv.* **2019**, *9*, 35895−35903.
(67) Gioia, C.; Lo Re, G.; Lawoko, M.; Berglund, L. A. Tunable thermosetting epoxies based on fractionated and well-characterized lignins. *J. Am. Chem. Soc.* **2018**, *140*, 4054−4061.
(68) Gioia, C.; Colonna, M.; Tagami, A.; Medina, L.; Sevastyanova, O.; Berglund, L. A.; Lawoko, M. Lignin-based epoxy resins: Unravelling the relationship between structure and material properties. *Biomacromolecules* **2020**, *21*, 1920−1928.
(69) Xu, Y.; Odelius, K.; Hakkarainen, M. Recyclable and flexible polyester thermosets derived from microwave-processed lignin. *ACS Appl. Polym. Mater.* **2020**, *2*, 1917−1924.
(70) Ribca, I.; Jawerth, M. E.; Brett, C. J.; Lawoko, M.; Schwartzkopf, M.; Chumakov, A.; Roth, S. V.; Johansson, M. Exploring the effects of different cross-linkers on lignin-based thermoset properties and morphologies. *ACS Sustainable Chem. Eng.* **2021**, *9*, 1692−1702.
(71) Truncali, A.; Ribca, I.; Yao, J.; Hakkarainen, M.; Johansson, M. Microwave-assisted fractionation and functionalization of technical lignin toward thermoset resins. *J. Appl. Polym. Sci.* **2023**, *140*, No. e54645.
(72) Gentile, G.; Mamone, M.; Rosso, C.; Amato, F.; Lanfrit, C.; Filippini, G.; Prato, M. Tailoring the Chemical Structure of Nitrogen-Doped Carbon Dots for Nano-Aminocatalysis in Aqueous Media. *ChemSusChem* **2023**, *16*, No. e202202399.
(73) Rosso, C.; Filippini, G.; Prato, M. Carbon Dots as Nano-Organocatalysts for Synthetic Applications. *ACS Catal.* **2020**, *10*, 8090−8105.
(74) Mondal, S.; Mandal, S.; Mondal, S.; Midya, S. P.; Ghosh, P. Photocatalytic Decarboxylation of Free Carboxylic Acids and Their Functionalization. *Chem. Commun.* **2024**, *60*, 9645−9658.
(75) Wallentin, C.-J.; Nguyen, J. D.; Finkbeiner, P.; Stephenson, C. R. J. Visible Light-Mediated Atom Transfer Radical Addition via Oxidative and Reductive Quenching of Photocatalysts. *J. Am. Chem. Soc.* **2012**, *134*, 8875−8884.

https://doi.org/10.1021/acssuschemeng.5c05307
ACS Sustainable Chem. Eng. 2025, 13, 12300−12310